J. Fluid Mech. (2002), *vol.* 453, *pp.* 263–287. © 2002 Cambridge University Press
DOI: 10.1017/S0022112001006942 Printed in the United Kingdom

Spatial variations of a passive tracer in a random wave field

By PETER B. WEICHMAN[1] AND ROMAN E. GLAZMAN[2]

[1]Blackhawk Geometrics, 301 Commercial Road, Suite B, Golden, CO 80401, USA

[2]Jet Propulsion Laboratory 300-323, California Institute of Technology, Pasadena, CA 91109, USA

(Received 28 August 2000 and in revised form 12 August 2001)

The effect of random wave fields on passive tracer spatial variations is studied. We derive a closed-form expression for the spatial autocorrelation function (or power spectrum) of the tracer fluctuations that is quantitatively accurate so long as wave field nonlinearities are small. The theory is illustrated for the case of long internal gravity waves in the ocean. We find that even if the (rear face of the) spectrum of the advecting velocity field is a pure power law, the tracer spectrum has two separate power law subranges. Most important to oceanographic applications, in the larger scale subrange, the effective horizontal compressibility of the wave velocity field becomes a dominant factor of the tracer variations. In such cases, the concentration spectrum becomes approximately proportional to the spectrum of the wave potential energy. The latter, which decays with increasing wavenumber much more rapidly than that known for two-dimensional eddy turbulence, is confirmed by satellite observations in wave-dominated ocean regions. As an additional confirmation of the theory, we demonstrate the occurrence of spectral peaks at wavenumbers corresponding to the semi-diurnal tide frequency.

1. Introduction

Spatial variations of sea surface temperature (SST), chlorophyll concentration and other tracers reflect, among other factors, a pattern of water motions in the upper ocean layer. For example, recent analyses of SST and chlorophyll concentration variations from long time series of satellite images reveal westward propagating features with spatial scales of several hundred kilometres, associated with baroclinic Rossby waves (Cipollini *et al.* 2001; Uz, Yoder & Osychny 2001). Manifestations of wave processes on much shorter time scales have also been observed (Weichman & Glazman 1999). However, theoretical studies of tracer variations have traditionally been focused on effects of eddy motions, which, as we discuss in detail later in this paper, led to erroneous interpretation of some observations. The present work analyses wave-induced variations and the joint effects of eddy and wave turbulence.

On all spatial scales greater than about 1 km, oceanic motions are essentially two-dimensional. On scales below about 100 km (in mid-latitude ocean regions) the kinetic energy spectrum of two-dimensional vortical motions is dominated by the direct inertial cascade of enstrophy. According to observations (Ogura 1952, 1962) and theoretical predictions (Kraichnan 1967, 1971; Batchelor 1969) the energy spectrum is given by $E(k) = C_\Omega \epsilon_\Omega^{2/3} k^{-3}$, where ϵ_Ω is the rate of enstrophy transfer in the spectral cascade and C_Ω is a universal constant. Present theory of turbulent transport then predicts the wavenumber spectrum of a spatially varying field of tracer concentration

https://doi.org/10.1017/S0022112001006942 Published online by Cambridge University Press

to be proportional to k^{-1} (see e.g. Gavrilin, Mirabel & Monin 1972; Saunders 1972; Kraichnan 1974). Many observations, however, yield much higher rates of spectral roll-off (see e.g. Gower, Denman & Holyer 1980; Deschamps, Frouin & Wald 1981; Barale & Trees 1987; Denman & Abbott 1994 and references therein) – as fast as k^{-3}. While various explanations have been suggested for these higher rates (see e.g. Charney 1971), none questioned whether two-dimensional eddy turbulence was an important dynamical factor in tracer variations on these short scales.

In the present work we study fluctuations originating from a different source of oceanic motions, namely those caused by random *waves*. While the formal theory presented here is general, the results will be specialized and applied in the end to the case of baroclinic inertia gravity (BIG) waves, since these waves represent one of two major classes of large-scale oceanic motions. The theory of passive tracer fluctuations in random wave fields presented in this paper should lead to better understanding of the observed patterns of tracer field concentration, including patchiness of biological fields.

As will be shown in § 4, in certain areas of the ocean BIG waves dominate the kinematics of the passive tracer field, at least on scales $10 \lesssim 2\pi/k \lesssim 500\,\mathrm{km}$. Such areas include many high-latitude regions in which eddy turbulence tends to be generally weak. It is well known (and has been confirmed by numerical models of ocean dynamics: see e.g. Maltrud *et al.* 1998) that the characteristic size of ocean eddies generated by ocean shear flows is comparable to the local Rossby radius of deformation. At high latitudes, the baroclinic Rossby radius is under 20 km. The energy of vortical turbulence is transferred from this range to larger scales through the inverse Kolmogorov-type spectral cascade, and the velocity spectrum behaves approximately as $k^{-5/3}$. The spectrum of BIG wave turbulence in the inverse cascade range behaves approximately as k^{-3} (Glazman 1996), and therefore grows at a more rapid rate as k decreases. Thus, if the energy of both the vortical and the wave motions is generated at high wavenumbers, the relative intensity of eddy turbulence at wavenumbers below the generation range (i.e. on scales greater than, say, 20 km) could drop well below that of BIG wave turbulence. Spatial variations of tracer fields may thus be affected by wave motions in a rather broad spectral range. The passive tracer spectrum measured by Gower *et al.* (1980) at 60°N latitude (where the Rossby radius is below 10 km), reproduced in figure 1, confirms this theory. This will be discussed in more detail and supported with more recent experimental data in § 4. In particular we will also show that observed spectra of chlorophyll-a concentration exhibit peaks at wavenumbers corresponding to semi-diurnal internal tide motions. The latter, in some ocean regions, represent the most prominent component of the BIG wave spectrum. The fact that the manifestation of internal tides in tracer fields has been overlooked in all previous experimental studies may be explained by the failure of existing theories to account for an impact of wave processes.

Passive scalar dynamics is governed by the transport equation

$$\partial_t q + \nabla \cdot (\boldsymbol{v} q) = 0 \tag{1.1}$$

for the concentration field $q(\boldsymbol{x}, t)$ advected by a random wave velocity field $\boldsymbol{v}(\boldsymbol{x}, t)$, which in this work will be taken to be spatially homogeneous and statistically stationary. Molecular diffusion, which is generally extremely small by comparison with turbulent diffusion, is neglected. It is commonly assumed that $\boldsymbol{v}$ is incompressible, $\nabla \cdot \boldsymbol{v} = 0$, but for wave fields, where one is interested mainly in horizontal variations, one is led naturally to effective *two-dimensional* descriptions – such as the shallow water equations – where the variation of the height of the free surface, or of isopycnal

https://doi.org/10.1017/S0022112001006942 Published online by Cambridge University Press

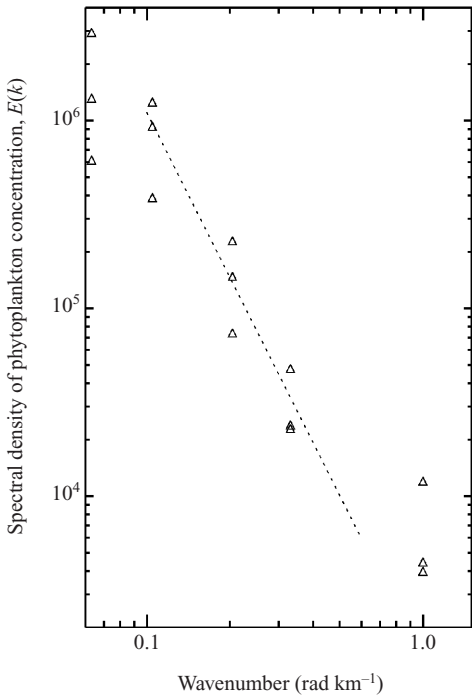


FIGURE 1. Power spectrum of chlorophyll-a fluctuations in a 180 km × 250 km ocean area south of Iceland, as reported in Gower *et al.* (1980) based on analysis of the Landsat multispectral imagery: triangles represent the experimental data; the dashed line is a $k^{-2.92}$ power law found as a least-squares fit to the data. (Reproduced courtesy of the authors.)

surfaces, leads to an effectively *compressible* horizontal velocity field $\boldsymbol{v}$. This property will turn out to be crucial to the strong influence of the wave field on the passive tracer concentration field: the compressional part of the wave field leads directly to fluctuations in the tracer concentration. In what follows all vectors will be restricted to the horizontal plane.

We will derive a closed-form solution for the autocorrelation function

$$R(\boldsymbol{x}-\boldsymbol{x}') = \langle q(\boldsymbol{x},t)q(\boldsymbol{x}',t)\rangle, \tag{1.2}$$

in which the average is over the appropriate ensemble of wave fields determined by the statistics of $\boldsymbol{v}$. In contrast to the classical problem of particle dispersion by eddy turbulence (reviewed e.g. in Monin & Yaglom 1971, chap. 5 and, more recently, in Klyatskin 1994) where no small parameter exists, wave-induced dispersion can be treated in a rigorous, controlled mathematical fashion (Herterich & Hasselmann 1982; Weichman & Glazman 1999, 2000). The derivation is based on the short-correlation approximation (reviewed, for example, in Piterbarg 1997) which, in the case of wave turbulence, is well justified: the time scale of typical wave oscillation periods (which is of the same order as the autocorrelation time scale for the fluctuating field $q(\boldsymbol{x},t)$) is much shorter than the time scale on which the evolution of $\langle q(\boldsymbol{x},t)\rangle$, $\langle q(\boldsymbol{x}_1,t)q(\boldsymbol{x}_2,t)\rangle$, etc. is observed.

We find also that even if the advecting velocity field has a pure power law turbulent spectrum, two separate power law subranges emerge in the tracer spectrum. It is found that at larger scales a linearized version of the passive tracer transport equation is

https://doi.org/10.1017/S0022112001006942 Published online by Cambridge University Press

valid, and leads to a power law dominated by the compressive part of the velocity field. However, at smaller scales, essentially nonlinear effects dominate, and a different power law obtains.

The closed-form expression for $R(\boldsymbol{r})$ obtained in this work is rather general and applies to either linear or nonlinear waves of an arbitrary nature – provided only that their nonlinearity is sufficiently weak. Conversely, the wave-induced diffusion studied by Herterich & Hasselmann 1982 and Weichman & Glazman 2000 is a second-order effect, associated with the wave nonlinearity, and vanishes for purely linear waves. Thus, the present effect is much stronger and easier to observe.

2. Theory of tracer fluctuations

2.1. *Quick derivation*

In order to understand, at the simplest possible level, the direct relationship between passive scalar statistics and statistics of the velocity field $\boldsymbol{v}$, consider the limit in which $\boldsymbol{v}$ is small. Let $\bar{q}$ be the overall mean tracer concentration, and assume that the fluctuating part $q(\boldsymbol{x})-\bar{q}$ is also small. The latter is actually an independent assumption since the size of $q-\bar{q}$ is set by initial conditions and may be large even if $\boldsymbol{v}$ is small. It will be lifted in the formal derivation in the next subsection. Linearizing (1.1) one obtains

$$\partial_t q = -\bar{q}\nabla\cdot\boldsymbol{v}. \tag{2.1}$$

In most cases the full three-dimensional field is incompressible, so one is assuming here a projected description in which only the horizontal velocity components are taken into account, and q has been vertically integrated. Such a description may be rigorously derived (Weichman & Glazman 2000), but we shall not discuss this procedure further here.

In real oceans the velocity $\boldsymbol{v}$ is actually composed of several different components coming from different ocean dynamic modes. Thus, gravity waves (which are of major interest here) usually propagate on a slowly evolving background of ocean currents, Rossby waves, and two-dimensional eddy turbulence. The time scales of such vortical (quasi-geostrophic) motions are of order weeks and longer, whereas the time scales of BIG waves (in mid- and high-latitude regions) are less than a day – as can be seen from dispersion curves for Rossby and inertia–gravity waves (see e.g. Gill 1982). This separation of time scales permits one to neglect slow variations in the tracer field occurring over time intervals of several wave periods, and hence to formally separate out the gravity wave contribution.

We therefore proceed as follows. Let $q_0(\boldsymbol{x})$ be the background eddy-induced concentration field, which one may think of as having been chosen from a statistical ensemble appropriate to quasi-geostrophic turbulence, but assumed fixed for the purposes of the wave calculation. Similarly, we drop all non-wave contributions to the velocity field $\boldsymbol{v}$ in (2.1), assuming them to be negligible on the above wave time scales. As a mathematical device we can take $q_0(\boldsymbol{x}) = q(\boldsymbol{x}, t = 0)$ as an initial condition, and assume that the wave field 'turns on' at $t = 0$. After several wave periods, the concentration field statistics will equilibrate to the stationary background-eddy-plus-wave form that we seek. It should be emphasized that this is only a mathematically convenient way of computing the combined statistics, and that $q_0(\boldsymbol{x})$ is not to be thought of as a physical initial condition.

We will see this equilibration property explicitly in the following computation of

https://doi.org/10.1017/S0022112001006942 Published online by Cambridge University Press

the covariance function. From (2.1) it follows immediately that

$$\begin{aligned}\Delta R(\boldsymbol{x}-\boldsymbol{x}',t) &\equiv \langle [q(\boldsymbol{x},t)-q_0(\boldsymbol{x})][q(\boldsymbol{x}',t)-q_0(\boldsymbol{x}')]\rangle \\ &= \bar{q}^2\int_0^t \mathrm{d}s_1\int_0^t \mathrm{d}s_2\langle \nabla\cdot\boldsymbol{v}(\boldsymbol{x},s_1)\nabla'\cdot\boldsymbol{v}(\boldsymbol{x}',s_2)\rangle \\ &= -\bar{q}^2\sum_{i,j}\partial_i\partial_j\int_0^t \mathrm{d}s_1\int_0^t \mathrm{d}s_2\, G_{ij}(\boldsymbol{x}-\boldsymbol{x}',s_1-s_2),\end{aligned} \tag{2.2}$$

in which the average is over the ensemble of velocity fields $\boldsymbol{v}$, and

$$G_{ij}(\boldsymbol{x}-\boldsymbol{x}',t-t') = \langle v_i(\boldsymbol{x},t)v_j(\boldsymbol{x}',t')\rangle \tag{2.3}$$

is the velocity correlator. Noting that for any function $f(t)$ that decays to zero rapidly for $|t|>\tau$, where τ is the decorrelation time of the wave field, one has

$$\begin{aligned}\int_0^t \mathrm{d}s\int_0^t \mathrm{d}s' f(s-s') &= \int_{-t}^t \mathrm{d}s(t-|s|)f(s) \\ &\to t\hat{f}(0)-\int_{-\infty}^{\infty}\mathrm{d}s|s|f(s),\end{aligned} \tag{2.4}$$

where $\hat{f}(\omega)$ is the Fourier transform of $f(t)$ and the last line follows for $|t|>\tau$. One then obtains

$$\Delta R(\boldsymbol{r},t)\to\Delta R(\boldsymbol{r})\equiv\bar{q}^2\sum_{i,j}\partial_i\partial_j\left[-t\hat{G}_{ij}(\boldsymbol{r},\omega=0)+\int_{-\infty}^{\infty}\mathrm{d}s|s|G_{ij}(\boldsymbol{r},s)\right]. \tag{2.5}$$

If $\hat{G}_{ij}(\boldsymbol{r},\omega=0)$ is non-zero, $\Delta R(\boldsymbol{r},t)$ has a linear time dependence. Realizing that $\hat{G}_{ij}(0,\omega)\equiv\hat{S}_{ij}(\omega)$ is just the frequency spectrum, the first term on the right-hand side of (2.5) acquires the following physical interpretation. As shown by Kubo (1963), in the short correlation time approximation, the turbulent diffusion tensor is given by $D_{ij}=\frac{1}{2}\hat{S}_{ij}(0)$. It can be shown that the form (2.8) below for the wave spectrum permits us to write $\hat{G}_{ij}(\boldsymbol{r},\omega=0)=2\alpha_{ij}(k_0\boldsymbol{r})D_{ij}$, where k_0 is the wavenumber that the dispersion relation $\omega(\boldsymbol{k})$ assigns to zero-frequency waves. The proportionality coefficients α_{ij}, appearing due to the spatial dependence of $\hat{G}_{ij}$, are bounded in magnitude by unity, and tend to unity as $\boldsymbol{r}\to\boldsymbol{0}$. Therefore, the linear time dependence in (2.5) describes the effects of diffusive decorrelation of the tracer field. In the full calculation below, we will see that this term actually arises from the formal expansion of a diffusion-type kernel $\mathscr{K}$ at short times. In the context of waves, the short correlation time approximation represents the leading term in an expansion of the diffusion tensor in powers of the small parameter u_0/c_0, i.e. the limit where the waves propagate through the tracer field much more quickly than the tracer particles themselves move (Herterich & Hasselmann 1982; Weichman & Glazman 2000). Now, for wave fields it transpires that $\hat{G}_{ij}(\boldsymbol{r},\omega)$, and $\hat{S}(\omega)$ in particular, vanish in a neighbourhood of $\omega=0$: for BIG waves the dispersion relation has a gap about $\omega=0$ given by the Coriolis parameter f, while for other types of waves $\omega=0$ corresponds to waves of infinite wavelength which do not exist in the ocean. The term linear in t therefore vanishes to lowest order and, after a transient of duration τ, the autocorrelation kernel relaxes to the time-independent form given by the second term in (2.5). This is precisely the statistical equilibration alluded to above, which is now seen to rely not only on the relative slowness of the eddy motions, but also on the subleading character of wave-induced diffusion. As shown by Herterich & Hasselmann (1982) (see also Weichman

https://doi.org/10.1017/S0022112001006942 Published online by Cambridge University Press

& Glazman 2000), the first non-vanishing contribution to the wave-induced diffusion tensor, and hence to a diffusive decorrelation term in (2.5), is of relative order $(u_0/c_0)^2$, and does not contribute to our leading-order calculation. Converting the time integral to a frequency integral, this may be expressed in the form

$$\Delta R(\boldsymbol{r}) = -\bar{q}^2 \sum_{i,j} \partial_i \partial_j \int \frac{\mathrm{d}\omega}{2\pi\omega^2} \hat{G}_{ij}(\boldsymbol{r},\omega), \tag{2.6}$$

and its spatial Fourier transform is

$$\Delta \hat{R}(\boldsymbol{k}) = \bar{q}^2 \sum_{i,j} \int \frac{\mathrm{d}\omega}{2\pi} \frac{k_i k_j}{\omega^2} \hat{\Phi}_{ij}(\boldsymbol{k},\omega), \tag{2.7}$$

in which $\hat{\Phi}_{ij}(\boldsymbol{k},\omega)$ is the full spatio-temporal Fourier transform of $G_{ij}(\boldsymbol{r},t)$. Now, for wave fields, $\hat{\Phi}_{ij}$ is non-zero only on surfaces determined by the wave dispersion relation $\omega(\boldsymbol{k})$:

$$\Phi_{ij}(\boldsymbol{k},\omega) = F_{ij}(\boldsymbol{k}) 2\pi\delta[\omega - \omega(\boldsymbol{k})] + F_{ji}(-\boldsymbol{k}) 2\pi\delta[\omega + \omega(-\boldsymbol{k})], \tag{2.8}$$

in which $F_{ij}(\boldsymbol{k})$ is the wavenumber spectrum. One therefore obtains finally the simple result

$$\Delta \hat{R}(\boldsymbol{k}) = \bar{q}^2 k^2 \left[\frac{F_L(\boldsymbol{k})}{\omega(\boldsymbol{k})^2} + \frac{F_L(-\boldsymbol{k})}{\omega(-\boldsymbol{k})^2} \right], \tag{2.9}$$

where $F_L(\boldsymbol{k}) = \sum_{i,j} \hat{k}_i \hat{k}_j F_{ij}(\boldsymbol{k})$ is the longitudinal (compressional) part of the wavenumber spectrum. The fact that only F_L enters is obvious in retrospect since the divergences imply that only the longitudinal part of $\boldsymbol{v}$ enters (2.2), and this exhibits the direct connection between the compressive nature of $\boldsymbol{v}$ and fluctuations in the tracer concentration. Of course, a more complete accounting for the (essentially nonlinear) advective terms in (1.1) – as is done in the next section – brings into play the transverse part of the velocity field, but nevertheless reproduces (2.9) at leading order. For an isotropic spectrum and dispersion relation, (2.9) reduces to

$$\Delta \hat{R}(\boldsymbol{k}) = 2\bar{q}^2 \frac{k^2 F_L(k)}{\omega(k)^2}. \tag{2.10}$$

Notice that (2.2) implies that the wave spectrum alters the tracer spectrum additively. The slow background field $q_0(\boldsymbol{x})$ introduced in (2.2) as the 'initial condition' is characterized by the spatial autocorrelation function

$$R_0(\boldsymbol{x} - \boldsymbol{x}') = [q_0(\boldsymbol{x}) q_0(\boldsymbol{x}')]_{\mathrm{av}}, \tag{2.11}$$

whose Fourier transform yields the power spectrum $\hat{R}_0(\boldsymbol{k})$. The 'initial field' $q_0(\boldsymbol{x})$ is therefore stochastic in character and $[\cdot]_{\mathrm{av}}$ denotes an appropriate ensemble average. For a large enough statistically homogeneous region $\mathscr{A}$ of area A, an equivalent operational definition is

$$R_0(\boldsymbol{r}) = \int_{\mathscr{A}} \frac{\mathrm{d}^d x}{A} q_0(\boldsymbol{x} + \boldsymbol{r}) q_0(\boldsymbol{x}), \tag{2.12}$$

in which the dimension is $d = 2$ for most applications, but we keep d general for computational convenience and generality. A full theory, which is beyond the scope of this work, would have to account simultaneously for the effects of the (possibly interacting) vortical eddy and wave field modes. However, as discussed earlier, vortical motions are slow, and hence we may ignore further vortical motions while considering

https://doi.org/10.1017/S0022112001006942 Published online by Cambridge University Press

the evolution of q on wave-related time scales. One sees from the above calculation that after a time of order the wave field decorrelation time τ, the full observed spectrum $\hat{R}(\boldsymbol{k})$, obtained from the Fourier transform of

$$R(\boldsymbol{x}-\boldsymbol{x}') = \langle [q(\boldsymbol{x},t)q(\boldsymbol{x}',t)]_{\mathrm{av}} \rangle, \tag{2.13}$$

indeed 'equilibrates' to a new steady state, given by the sum

$$\hat{R}(\boldsymbol{k}) = R_0(\boldsymbol{k}) + \Delta\hat{R}(\boldsymbol{k}). \tag{2.14}$$

The additive nature of this spectral renormalization means, in particular, that observation of the effects of waves on passive tracer fluctuations in any particular part of the spectrum requires that the wave energy spectrum be of the same order or larger than the eddy energy spectrum. If such is the case, (2.14) then provides an explanation for the more rapid than expected fall-off in the observed spectrum of concentration field fluctuations: see § 3 below for a more detailed discussion. We emphasize again that only the combined time-independent correlation function R will be physically observed. The appearance here of R_0 as an initial condition at $t = 0$ is only a mathematical device that allows us to conveniently compute ΔR.

2.2. *Formal theory*

In order to confirm the content of (2.9) and (2.14) we turn to a full theory of passive tracer fluctuations. This will allow us to evaluate the range of validity of the quick derivation and to understand the origin of any corrections. The results derived in this subsection will be valid for an initial $q_0(\boldsymbol{x})$ with arbitrarily large fluctuations, so long as $\boldsymbol{v}$ is at most weakly nonlinear.

The formal theory (Weichman & Glazman 2000) is based on a Lagrangian representation of the passive scalar dynamics. Excellent reviews of this approach can be found in Piterbarg (1997), Bennett (1996) and references therein. Let $\boldsymbol{Z}_{xt}(s)$ be the (Lagrangian) position of a fluid particle at time s, provided this particle has been (or will be) found at point $\boldsymbol{x}$ at time t. The tracer concentration field may then be represented in the form (Weichman & Glazman 2000; Bennett 1996)

$$q(\boldsymbol{x},t) = \int \mathrm{d}^d x'\, q_0(\boldsymbol{x}')\delta[\boldsymbol{x} - \boldsymbol{Z}_{x'0}(t)] = q_0[\boldsymbol{Z}_{xt}(0)]\det[\partial \boldsymbol{Z}_{xt}(0)/\partial \boldsymbol{x}], \tag{2.15}$$

where the Jacobian determinantal factor accounts for the 'compressibility' of the horizontal velocity field $\boldsymbol{v}$ in the horizontal plane $\boldsymbol{x}$, i.e. for the fact that $\nabla \cdot \boldsymbol{v} \neq 0$.

The calculation proceeds as follows. Using the random walk representation, the double-ensemble averaged equal-time autocorrelation function is given by

$$\begin{aligned} R(\boldsymbol{x}-\boldsymbol{x}',t) &= \langle [q(\boldsymbol{x},t)q(\boldsymbol{x}',t)]_{\mathrm{av}} \rangle \\ &= \int \mathrm{d}^d y \int \mathrm{d}^d y' [q_0(\boldsymbol{y})q_0(\boldsymbol{y}')]_{\mathrm{av}} \langle \delta[\boldsymbol{x} - \boldsymbol{Z}_{y0}(t)]\delta[\boldsymbol{x}' - \boldsymbol{Z}_{y'0}(t)] \rangle \\ &= \int \frac{\mathrm{d}^d k}{(2\pi)^d} \int \frac{\mathrm{d}^d k'}{(2\pi)^d} \int \mathrm{d}^d y \int \mathrm{d}^d y'\, R_0(\boldsymbol{y}-\boldsymbol{y}') \\ &\quad \times \exp(\mathrm{i}\boldsymbol{k}\cdot(\boldsymbol{x}-\boldsymbol{y}) + \mathrm{i}\boldsymbol{k}'\cdot(\boldsymbol{x}'-\boldsymbol{y}'))\exp(-\lambda(\boldsymbol{k},\boldsymbol{k}';\boldsymbol{y}-\boldsymbol{y}',t)), \end{aligned} \tag{2.16}$$

where in the last line the Fourier representation of the delta-functions has been used and, letting $\Delta\boldsymbol{Z}_{y0}(t) \equiv \boldsymbol{Z}_{y0}(t) - \boldsymbol{y}$, we define the characteristic functional

$$\lambda(\boldsymbol{k},\boldsymbol{k}';\boldsymbol{y}-\boldsymbol{y}',t) \equiv -\ln\langle \exp(-\mathrm{i}\boldsymbol{k}\cdot\Delta\boldsymbol{Z}_{y0}(t) - \mathrm{i}\boldsymbol{k}'\cdot\Delta\boldsymbol{Z}_{y'0}(t)) \rangle. \tag{2.17}$$

https://doi.org/10.1017/S0022112001006942 Published online by Cambridge University Press

Changing variables to $\boldsymbol{r}' = \boldsymbol{y} - \boldsymbol{y}'$ and $\boldsymbol{Y} = (\boldsymbol{y} + \boldsymbol{y}')/2$, one sees that the only dependence of the integrand in (2.16) on the centre-of-mass variable $\boldsymbol{Y}$ is through an exponential factor $\exp(\mathrm{i}(\boldsymbol{k} + \boldsymbol{k}') \cdot \boldsymbol{Y})$. The $\boldsymbol{Y}$-integration therefore produces a delta-function enforcing $\boldsymbol{k} + \boldsymbol{k}' = \boldsymbol{0}$. One then obtains

$$R(\boldsymbol{r}) = \int \mathrm{d}^d r'\, R_0(\boldsymbol{r}')\mathscr{K}(\boldsymbol{r}, \boldsymbol{r}', t), \tag{2.18}$$

in which the integration kernel $\mathscr{K}$ is given by

$$\mathscr{K}(\boldsymbol{r}, \boldsymbol{r}', t) = \int \frac{\mathrm{d}^d k}{(2\pi)^d} \exp(\mathrm{i}\boldsymbol{k} \cdot (\boldsymbol{r} - \boldsymbol{r}') - \lambda(\boldsymbol{k}, -\boldsymbol{k}; \boldsymbol{r}', t)). \tag{2.19}$$

Noting that $\hat{R}_0(\boldsymbol{k}) = (2\pi)^d \bar{q}^2 \delta(\boldsymbol{k}) + \tilde{R}_0(\boldsymbol{k})$ and $\hat{R}(\boldsymbol{k}) = (2\pi)^d \bar{q}^2 \delta(\boldsymbol{k}) + \tilde{R}(\boldsymbol{k})$ contain delta-function pieces coming from the fact that their real-space forms asymptote to $\bar{q}^2$ for large r, in Fourier space one obtains the equivalent form

$$\tilde{R}(\boldsymbol{k}) = \bar{q}^2 \hat{\mathscr{K}}(\boldsymbol{k}, \boldsymbol{0}, t) + \exp(-\lambda_\infty(\boldsymbol{k}, -\boldsymbol{k}, t))\tilde{R}_0(\boldsymbol{k}) + \int \frac{\mathrm{d}^d k'}{(2\pi)^d} \hat{\mathscr{K}}(\boldsymbol{k}, \boldsymbol{k}', t)\tilde{R}_0(\boldsymbol{k}') \tag{2.20}$$

in which $\hat{\mathscr{K}}$ is given by

$$\hat{\mathscr{K}}(\boldsymbol{k}, \boldsymbol{k}', t) = \int \mathrm{d}^d r' \exp(-\mathrm{i}(\boldsymbol{k} - \boldsymbol{k}') \cdot \boldsymbol{r}') \left[\exp(-\lambda(\boldsymbol{k}, -\boldsymbol{k}; \boldsymbol{r}', t)) - \exp(-\lambda_\infty(\boldsymbol{k}, -\boldsymbol{k}; t))\right]. \tag{2.21}$$

The subtraction

$$\begin{aligned} \exp(-\lambda_\infty(\boldsymbol{k}, -\boldsymbol{k}, t)) &= \lim_{|\boldsymbol{r}'| \to \infty} \exp(-\lambda_\infty(\boldsymbol{k}, -\boldsymbol{k}; \boldsymbol{r}', t)) \\ &= |\langle \exp(-\mathrm{i}\boldsymbol{k} \cdot \Delta\boldsymbol{Z}_{\boldsymbol{y}0}(t)) \rangle|^2 \end{aligned} \tag{2.22}$$

is required to eliminate the corresponding delta-function terms in $\hat{\mathscr{K}}$ itself. We will see that the quick derivation result of the previous subsection emerges in an appropriate limit from the first two terms in (2.20).

To evaluate $\mathscr{K}$ more explicitly an approximate scheme for computing λ must be developed. As shown in Weichman & Glazman (2000), for wave fields there exists a well-defined perturbation theory in the small parameter u_0/c_0, where $u_0 = \sqrt{\langle \boldsymbol{v}^2 \rangle}$ is the characteristic particle velocity and c_0 is the characteristic phase speed of the waves. Under typical ocean conditions one finds $u_0/c_0 = O(10^{-1})$. The perturbation theory is implemented first by performing a cummulant expansion in powers of $\Delta\boldsymbol{Z}$:

$$\begin{aligned} \lambda(\boldsymbol{k}, -\boldsymbol{k}; \boldsymbol{y} - \boldsymbol{y}', t) = {} & \mathrm{i}\langle \boldsymbol{k} \cdot [\Delta\boldsymbol{Z}_{\boldsymbol{y}0}(t) - \Delta\boldsymbol{Z}_{\boldsymbol{y}0}(t)] \rangle \\ & + \tfrac{1}{2} \langle \{\boldsymbol{k} \cdot [\Delta\boldsymbol{Z}_{\boldsymbol{y}0}(t) - \Delta\boldsymbol{Z}_{\boldsymbol{y}0}(t)]\}^2 \rangle_c + O[(ku_0 t)^3], \end{aligned} \tag{2.23}$$

in which the subscript c indicates that the product of the averages should be subtracted. The first term represents the mean relative drift of two particles a distance $\boldsymbol{r}'$ apart. Since we are considering a homogeneous situation, so that $\langle \Delta\boldsymbol{Z}_{\boldsymbol{y}0}(t) \rangle$ is independent of $\boldsymbol{y}$, this term vanishes identically. Defining the Lagrangian correlator

$$\Gamma_{ij}(\boldsymbol{y} - \boldsymbol{y}', t) = \langle [\Delta\boldsymbol{Z}_{\boldsymbol{y}0}(t) - \Delta\boldsymbol{Z}_{\boldsymbol{y}'0}(t)]_i [\Delta\boldsymbol{Z}_{\boldsymbol{y}0}(t) - \Delta\boldsymbol{Z}_{\boldsymbol{y}'0}(t)]_j \rangle \tag{2.24}$$

and neglecting all higher-order terms in λ (which is valid for small $ku_0\tau$, i.e. on length scales larger than the typical distance travelled by a tracer particle in a typical wave

https://doi.org/10.1017/S0022112001006942 Published online by Cambridge University Press

period – roughly a factor u_0/c_0 times the dominant wavelength), one obtains

$$\mathscr{K}(\boldsymbol{r},\boldsymbol{r}',t) = \int \frac{\mathrm{d}^d k}{(2\pi)^2} \exp(\mathrm{i}\boldsymbol{k}\cdot(\boldsymbol{r}-\boldsymbol{r}')) \exp(-\tfrac{1}{2}\sum_{i,j} \Gamma_{ij}(\boldsymbol{r}',t)k_i k_j)$$
$$= \frac{\exp\left(-\frac{1}{2}\sum_{i,j}\Gamma^{-1}_{ij}(\boldsymbol{r}',t)(\boldsymbol{r}'-\boldsymbol{r})_i(\boldsymbol{r}'-\boldsymbol{r})_j\right)}{\sqrt{\det[2\pi\boldsymbol{\Gamma}(\boldsymbol{r}',t)]}}, \tag{2.25}$$

in which Γ^{-1}_{ij} is the inverse of the matrix Γ_{ij}. The kernel $\mathscr{K}$ therefore reflects explicitly the Lagrangian autocorrelations. The theory presented in Weichman & Glazman (2000) now also allows one to evaluate Γ_{ij} perturbatively in terms of Eulerian velocity correlators of the wave field. First, one has the exact defining relation

$$\Delta\boldsymbol{Z}_{\boldsymbol{y}0}(t) = \int_0^t \mathrm{d}s\, \boldsymbol{v}(\boldsymbol{Z}_{\boldsymbol{y}0}(s),s). \tag{2.26}$$

Second, if $\Delta\boldsymbol{Z}_{\boldsymbol{y}0}(t) = O(u_0 t)$ is small compared to the typical length scale of variation of $\boldsymbol{v}(\boldsymbol{y},t)$, i.e. if $u_0 t/c_0 t_0$ is small, one may simply replace $\boldsymbol{v}(\boldsymbol{Z}_{\boldsymbol{y},0}(s),s)$ by its Eulerian counterpart $\boldsymbol{v}(\boldsymbol{y},s)$, with corrections of relative order u_0/c_0 (which may be computed in a gradient expansion of $\boldsymbol{v}$: Weichman & Glazman 2000). The length scale $\boldsymbol{v}$ is given by the typical wavelength $\lambda_0 = c_0 t_0$, where t_0 is the wave period, and this condition will be valid if t is not too much larger than t_0. We will see below that we only need t up to the decorrelation time τ, which is indeed typically of the same order as t_0. Thus, in terms of the Eulerian velocity correlator (2.3), one obtains to lowest order

$$\Gamma_{ij}(\boldsymbol{r},t) = \int_0^t \mathrm{d}s \int_0^t \mathrm{d}s' [2G_{ij}(\boldsymbol{0},s-s') - G_{ij}(\boldsymbol{r},s-s') - G_{ij}(-\boldsymbol{r},s-s')], \tag{2.27}$$

with corrections of relative $O(u_0^2/c_0^2)$. Using (2.4) one obtains

$$\Gamma_{ij}(\boldsymbol{r},t) \to t[\hat{G}_{ij}(\boldsymbol{0},0) - \hat{G}_{ij}(\boldsymbol{r},0)] - \int_{-\infty}^{\infty} \mathrm{d}s|s|[G_{ij}(\boldsymbol{0},s) - G_{ij}(\boldsymbol{r},s)] + (i\leftrightarrow j), \quad t>\tau. \tag{2.28}$$

The term linear in t once again vanishes for wave turbulence, and after a transient of duration τ, the autocorrelation kernel relaxes to the time-independent form

$$\mathscr{K}_\infty(\boldsymbol{r},\boldsymbol{r}') \equiv \mathscr{K}(\boldsymbol{r},\boldsymbol{r}',\infty) = \frac{\exp\left(-\frac{1}{2}\sum_{i,j}\gamma^{-1}_{ij}(\boldsymbol{r}')(\boldsymbol{r}'-\boldsymbol{r})_i(\boldsymbol{r}'-\boldsymbol{r})_j\right)}{\sqrt{\det[2\pi\boldsymbol{\gamma}(\boldsymbol{r}',t)]}} \tag{2.29}$$

$$\hat{\mathscr{K}}_\infty(\boldsymbol{k},\boldsymbol{k}') = \int \mathrm{d}^d r' \exp(-\mathrm{i}(\boldsymbol{k}-\boldsymbol{k}')\cdot\boldsymbol{r}') \left[\exp\left(-\tfrac{1}{2}\sum_{i,j}\gamma_{ij}(\boldsymbol{r}')k_i k_j\right) - \exp\left(-\tfrac{1}{2}\sum_{i,j}\gamma_{ij}(\infty)k_i k_j\right)\right], \tag{2.30}$$

with

$$\gamma_{ij}(\boldsymbol{r}) = -\int_{-\infty}^{\infty} \mathrm{d}s|s|[G_{ij}(\boldsymbol{0},s) - G_{ij}(\boldsymbol{r},s)] + (i\leftrightarrow j)$$
$$= \int_{-\infty}^{\infty} \frac{\mathrm{d}\omega}{2\pi\omega^2}[\hat{S}_{ij}(\omega) - \hat{G}_{ij}(\boldsymbol{r},\omega)] + (i\leftrightarrow j)$$
$$= 2\int \frac{\mathrm{d}^d k}{(2\pi)^d} \frac{F_{ij}(\boldsymbol{k}) + F_{ji}(\boldsymbol{k})}{\omega(\boldsymbol{k})^2}[1-\cos(\boldsymbol{k}\cdot\boldsymbol{r})]. \tag{2.31}$$

https://doi.org/10.1017/S0022112001006942 Published online by Cambridge University Press

and therefore

$$\gamma_{ij}(\infty) = \int_{-\infty}^{\infty} \frac{\mathrm{d}\omega}{2\pi\omega^2}[\hat{S}_{ij}(\omega) + \hat{S}_{ji}(\omega)]$$
$$= 2\int \frac{\mathrm{d}^d k}{(2\pi)^d} \frac{F_{ij}(\boldsymbol{k}) + F_{ji}(\boldsymbol{k})}{\omega(\boldsymbol{k})^2}. \tag{2.32}$$

The Fourier transform of $\tilde{\gamma}_{ij}(\boldsymbol{r}) \equiv \gamma_{ij}(\infty) - \gamma_{ij}(\boldsymbol{r})$ is then

$$\tilde{\gamma}_{ij}(\boldsymbol{k}) = \left[\frac{F_{ij}(\boldsymbol{k}) + F_{ji}(\boldsymbol{k})}{\omega(\boldsymbol{k})^2} + \frac{F_{ij}(-\boldsymbol{k}) + F_{ji}(-\boldsymbol{k})}{\omega(-\boldsymbol{k})^2}\right]. \tag{2.33}$$

As alluded to earlier, higher-order corrections actually produce a linear time dependence with corrected diffusion coefficient of relative order (u_0^2/c_0^2) (Herterich & Hasselmann 1982; Weichman & Glazman 2000) which then produces diffusive decorrelation on a much larger time scale of $O(c_0^2\tau/u_0^2)$.

2.3. *Calculation of spectral renormalization*

The effect of the kernel $\mathscr{K}$ on the background spectrum $\hat{R}_0(\boldsymbol{k})$ depends crucially on the range of k that one is considering. The result (2.30) is valid so long as k^2 times the leading (relative $O(u_0^2/c_0^2)$) corrections to (2.27) are small, i.e. if $k^2u_0^4\tau^2/c_0^2 \sim (k\lambda_0)^2(u_0/c_0)^4 \ll 1$, where $\lambda_0 \sim c_0t_0$ is a characteristic length determined by the spectral peak frequency. Thus k should be small compared to $c_0^2/u_0^2\lambda_0 \sim c_0/u_0d_0$, where $d_0 = u_0t_0$ is the characteristic distance travelled by the tracer particle in a dominant wave period. Since c_0^2/u_0^2 is typically of order 10^2, this puts the upper bound on allowed k nearly two decades into the inertial range of $\boldsymbol{v}$. Due to the complexity of the relations (2.18) and (2.20), however, the inertial-range power law spectra of $\boldsymbol{v}$ do not lead immediately in the same range to simple power law spectra for q. Rather, as we now demonstrate, although the inertial-range behaviour of $\boldsymbol{v}$ determines that of q, different spectral power laws for q are exhibited in different ranges of k.

Let us first rederive (2.14). Suppose that k is sufficiently small that $k^2\gamma_{ij}(\boldsymbol{r})$ is also small, i.e. $k^2(u_0\tau)^2 \sim (k\lambda_0)^2(u_0/c_0)^2 \ll 1$. This requires that k be small compared to $c_0/u_0\lambda_0 \sim 1/d_0$, limiting it to less than a decade into the inertial range. One may then expand $\hat{\mathscr{K}}_\infty(\boldsymbol{k},\boldsymbol{k}')$ in the form

$$\hat{\mathscr{K}}_\infty(\boldsymbol{k},\boldsymbol{k}') = \int \mathrm{d}^d r' \exp(-\mathrm{i}(\boldsymbol{k}-\boldsymbol{k}')\cdot\boldsymbol{r}')\left[\tfrac{1}{2}\sum_{i,j}\tilde{\gamma}_{ij}(\boldsymbol{r}')k_ik_j + O[(u_0\tau k)^4]\right]$$
$$= \tfrac{1}{2}\sum_{i,j}\tilde{\gamma}_{ij}(\boldsymbol{k}-\boldsymbol{k}')k_ik_j[1 + O(u_0^2\tau^2k^2)]. \tag{2.34}$$

Inserting this into (2.20), the first term reduces precisely to (2.9) and one obtains (2.14), but now with leading corrections:

$$\tilde{R}(\boldsymbol{k}) = \Bigg\{\tilde{R}_0(\boldsymbol{k}) + \Delta\hat{R}(\boldsymbol{k})$$
$$- \tfrac{1}{2}R_0(\boldsymbol{k})\sum_{i,j}k_ik_j\left[\gamma_{ij}(\infty)\tilde{R}_0(\boldsymbol{k}) - \int\frac{\mathrm{d}^d k'}{(2\pi)^d}\tilde{\gamma}_{ij}(\boldsymbol{k}-\boldsymbol{k}')\tilde{R}_0(\boldsymbol{k}')\right]\Bigg\}[1 + O(k^2u_0^2\tau^2)]. \tag{2.35}$$

https://doi.org/10.1017/S0022112001006942 Published online by Cambridge University Press

The original quick derivation was based on the assumption that fluctuations in q were small compared to the mean $\bar{q}$, i.e. that $\tilde{R}_0(\boldsymbol{k}) \ll \bar{q}^2$. Under this condition the second line of (2.35) is small compared to the first two terms, and (2.14) is rigorously recovered.

We remark in passing that the k-space approximation used in (2.34) may also be implemented in the real-space form (2.29). The small-k limit is equivalent to the limit where r is sufficiently large that $\gamma_{ij}(\boldsymbol{r}')$ is slowly varying over the range of $\boldsymbol{r}'$ for which the exponential numerator in (2.29) is not vanishingly small, i.e. the limit where the replacement of $\gamma_{ij}(\boldsymbol{r}')$ by $\gamma_{ij}(\boldsymbol{r})$ in the exponential is permitted. The real-space form of (2.35) is then obtained by making this replacement and then performing a second-order Taylor expansion of the determinant denominator of the right-hand side of (2.29) in the difference $\boldsymbol{r}' - \boldsymbol{r}$.

Suppose next that $1/d_0 \leqslant k \ll c_0/u_0 d_0$, so that the Taylor expansion of the exponential is no longer appropriate. In the real-space form this means that $\boldsymbol{r}$ is small enough that $\gamma_{ij}(\boldsymbol{r}')$ varies substantially over the range where the exponential numerator in (2.29) is non-vanishing. The analysis in this regime is most simply carried out directly in real space. To simplify the calculations we will consider only the case where the spectrum of $\boldsymbol{v}$ is isotropic, and $\gamma_{ij}(\boldsymbol{r}) = \gamma(r)\delta_{ij}$ is diagonal. Isotropy allows a more general form with independent longitudinal and transverse components, $\gamma_L(r)$ and $\gamma_T(r)$, but we treat here only the simplest case $\gamma_T = \gamma_L$. One obtains then

$$\mathscr{K}_\infty(r', |\boldsymbol{r}' - \boldsymbol{r}|) = \frac{\exp(-|\boldsymbol{r}' - \boldsymbol{r}|^2/2\gamma(r'))}{[2\pi\gamma(r')]^{d/2}}. \tag{2.36}$$

Since $\gamma(r')$ vanishes as $r' \to 0$ this kernel becomes a delta-function in $\boldsymbol{r}$ at this point. For r' away from the origin, $\mathscr{K}$ roughly averages $R_0(r')$ over an area of radius $\sqrt{\gamma}$. The behaviour of the Fourier spectrum $\hat{R}_0(k)$ at large k is reflected in the behaviour of $R_0(r)$ at small r. Thus, if the spectrum decays rapidly, $R_0(r)$ will have a Taylor expansion in r^2 about the origin. If the spectrum decays as a slow power law, $k^{-(d+\alpha)}$ (with dimension $d = 2$ in the present case), then one will have a leading behaviour of the form $R_0(r) = R_0(0)[1 - Ar^\alpha]$ (with $\alpha < 0$ permitted). Similarly, if the BIG wave spectrum decays as a slow power law, one will have the leading behaviour $\gamma(r) = Br^\beta$ with, typically, $0 < \beta < 2$.

Given the two exponents α and β, the final question we address is the resulting leading behaviour $R(r) = R(0)[1 - Cr^\mu]$. In particular, what is the function $\mu(\alpha, \beta)$? This function can be inferred from the analysis of the integral (A 1) in Appendix A with the identification $\sigma = -\alpha - d(2 - \beta)/2$. In addition to analytic contributions to $R(r)$, there is a leading non-analytic contribution with exponent

$$\mu(\alpha, \beta) = -2\sigma/\beta = 2(\alpha + d)/\beta - d. \tag{2.37}$$

This exponent then translates into a large-k Fourier space (angular integrated) spectral form $\sim k^{-p}$ with

$$p(\alpha, \beta) = \mu(\alpha, \beta) + d - (d - 1) = 2(\alpha + d)/\beta + 1 - d. \tag{2.38}$$

3. Implications of the general theory

Equations (2.14) and (2.20) are the basic results of this paper. The first term on the right-hand side of (2.20) represents the effect of the compressional component of the wave velocity field (as in the absence of pre-existing, vortical motions), while the

https://doi.org/10.1017/S0022112001006942 Published online by Cambridge University Press

third term describes interactions of eddy and wave motions. In the absence of wave motion, the second term reduces to the spectrum of tracer variations, $\tilde{R}_0(\boldsymbol{k})$, caused by eddy turbulence and the other two terms disappear.

When the wave spectrum is broad – as in the case of wave turbulence – a search for possible power laws in the tracer spectrum yields particularly interesting results. One sees that even if the initial concentration field correlator $R_0(r)$ is analytic (corresponding to rapid decay of $\tilde{R}_0(k)$ for large k), indicating a smooth initial condition, these equations will produce non-trivial power law behaviour in $\hat{R}(k)$. Considering first the range $k\lambda_0 < c_0/u_0$ where (2.14) is valid, if $F(k) \approx F_0 k^{-d-q}$ and $\omega(k) \approx C_0 k^{\zeta}$ in this range, then the angle-integrated tracer spectrum will vary as

$$k^{d-1}\Delta\hat{R}(k) \sim k^{1-q-2\zeta}, \quad k\lambda_0 < c_0/u_0. \tag{3.1}$$

Now, as discussed later in § 4, the (angle-integrated) BIG wave wavenumber spectrum $k^{d-1}F(k)$ (with $d = 2$) is observed to vary as $k^{-4/3}$ for $ck \gg f$. This corresponds to $F(k) \sim k^{-7/3}$, and hence $q = 1/3$. In this range one has simply $\omega(k) \approx ck$, i.e. $\zeta = 1$, and we then obtain $k^{d-1}\Delta\hat{R}(k) \sim k^{-p}$, with $p = 4/3$. Here the wave dynamics are assumed to be dominated by the direct energy cascade. However, the BIG wave spectrum also includes an inverse cascade (of *wave action*) range that yields $k^{d-1}F(k) \sim k^{-3}$, corresponding to $q = 2$ and hence $k^{d-1}\Delta\hat{R}(k) \sim k^{-p}$ with $p = 3$. Since the wavenumber range over which most of the external energy/action input occurs is not known, the precise wavenumber separating the direct and inverse cascades is not known. Theoretically, the k^{-3} range may extend to length scales shorter than 10 km – the characteristic size of two-dimensional eddies in high-latitude ocean regions (which is comparable to the local baroclinic Rossby radius of deformation). However, observational data on BIG wave spatial spectra (of either sea surface height or ocean currents) in this short-scale range are unavailable. Clearly, depending upon the precise ocean conditions, and hence the exact balance between the various terms entering the determination of $\hat{R}(k)$, the present theory allows an effective tracer spectral exponent anywhere within the observed range $1 \leqslant p \leqslant 3$.

Consider next the range $c_0/u_0 < \lambda_0 k < (c_0/u_0)^2$ in which (2.37) is valid. This equation will produce a series of singularities corresponding to non-negative even integer values of α. The leading singularity (corresponding to $\alpha = 0$) takes the form (in $d = 2$)

$$\mu(0,\beta) = 4/\beta - 2, \quad p(0,\beta) = 4/\beta - 1 \tag{3.2}$$

corresponding to a Fourier space spectral decay $k^{-(d+\mu)} = k^{-4/\beta}$. Interestingly, the more fractal like the wave velocity field spectrum is (the smaller the value of β), the less fractal like (the steeper the fall-off of) the passive tracer spectrum. The $1/k$ theoretical (angular integrated) spectrum alluded to in the introduction corresponds to the case of a logarithmic divergence in $R_0(r)$ as $r \to 0$. This yields, effectively, $\alpha = 0$ and (3.2) is predicted to be valid, up to possible logarithmic corrections. A value $\beta = 1$ would then produce a wave-field renormalized k^{-3} spectrum, consistent with observations.

Let us now derive a form for β for a given behaviour of the frequency or wavenumber spectrum. The full wavenumber–frequency spectrum for a general wave field is given by (2.8) in which the dispersion relation is $\omega(\boldsymbol{k}) = \sqrt{f^2 + c^2k^2}$ for BIG waves, where $f = 2\Omega\sin(\phi)$ is the Coriolis parameter (Ω being the Earth's rotation frequency and ϕ being the latitude). In the isotropic approximation in which we work, we assume $F_{ij}(\boldsymbol{k}) = (1/d)F(k)\delta_{ij}$ and consider only isotropic $\omega(\boldsymbol{k}) = \omega(k)$ so that the

https://doi.org/10.1017/S0022112001006942 Published online by Cambridge University Press

total kinetic energy spectrum (the trace of Φ_{ij}) is

$$\Phi(k,\omega) = 2\pi F(k)\{\delta[\omega-\omega(k)]+\delta[\omega+\omega(k)]\}. \tag{3.3}$$

From (2.36) and (A 9) one then obtains

$$\begin{aligned}\gamma(r) &= \frac{2}{d}\int\frac{\mathrm{d}^d k}{(2\pi)^d}\int\frac{\mathrm{d}\omega}{2\pi\omega^2}\Phi(k,\omega)[1-\mathrm{e}^{\mathrm{i}\boldsymbol{k}\cdot\boldsymbol{r}}]\\ &= \frac{4}{d}\int\frac{\mathrm{d}^d k}{(2\pi)^d}\frac{F(k)}{\omega(k)^2}\left[1-\mathrm{e}^{\mathrm{i}\boldsymbol{k}\cdot\boldsymbol{r}}\right]\end{aligned} \tag{3.4}$$

Thus, if $F(k)\approx F_0 k^{-d-q}$ and $\omega(k)\approx C_0 k^{\zeta}$ for large k, $\gamma(r)$ will have a singular term varying as

$$\gamma_{\mathrm{sing}}(r) = \gamma_s r^{q+2\zeta}, \quad \gamma_s = \frac{2^{2-q-2\zeta}F_0}{d(4\pi)^{d/2}C_0^2}\frac{\Gamma\left(-\zeta-\frac{1}{2}q\right)}{\Gamma\left(\zeta+\frac{1}{2}(d+q)\right)}, \tag{3.5}$$

in which (A 9) and relation 6.561.14 (p. 684) of Gradshteyn & Rhyzhik (1981) has been used.

If $q+2\zeta<2$ then this will be the leading term, and one immediately identifies $\beta = q+2\zeta$. On the other hand, if $q+2\zeta>2$ then this singular term will be subleading, and $\gamma(r)$ will have a leading r^2 term given by

$$\gamma(r) = \gamma_2 r^2 + \gamma_s r^{q+2\zeta} + O(r^4), \quad \gamma_2 = \frac{4}{d^2}\int\frac{\mathrm{d}^d k}{(2\pi)^d}\frac{k^2 F(k)}{\omega(k)^2}. \tag{3.6}$$

In this case one would then identify $\beta=2$, and infer the general relation

$$\beta = \min\{q+2\zeta, 2\}. \tag{3.7}$$

For $q>0$ and $\zeta=1$ one has $2\zeta+q>2$ and we infer that $\beta=2$ in all the cases discussed above. The results in Appendix A (case (vi)) then imply that $\mu=\alpha$: the initial spectrum is unrenormalized in this range of larger k.

We conclude that the effects of BIG waves on the passive tracer spectrum are expected to be strongest only in the smaller k range where (2.10) and (2.14) are valid. For BIG waves the spectral peak is at the Coriolis frequency f. The characteristic length $\lambda_0 \sim c/f \equiv R$ is then determined by the Rossby radius R. At mid-latitudes $R\sim$ 20–40 km. The condition for the validity of (2.10) and (2.14) is then that $k<c_0/u_0 R$, i.e. that length scales $\lambda>2\pi(u_0/c_0)R\sim$ 10–20 km be considered.

As mentioned earlier, a prominent feature of the BIG wave spectrum (appearing in ocean regions where internal tides are generated as a result of barotropic tide scattering by sharp variations in ocean floor topography), is the semi-diurnal tide peak. The dispersion law for BIG waves yields the wavenumber k_T of semi-diurnal tides in the form

$$k_T = \frac{2\Omega}{c}\cos(\phi). \tag{3.8}$$

For typical Kelvin wave speeds c in the range 2–5 m s^{-1}, the wavelength of baroclinic tides varies, depending on the latitude, between 150 and 400 km. We therefore expect the presence of a local peak in the power spectrum of tracer variations in the corresponding wavenumber range.

https://doi.org/10.1017/S0022112001006942 Published online by Cambridge University Press

4. Comparison with experimental data

Detailed comparison of theory with observations has recently become possible due to the accumulation of large volumes of high-quality satellite data on ocean tracer distributions and underlying ocean dynamics. As a most relevant and readily available characteristic of the latter, we shall discuss the wavenumber spectrum of sea surface height (SSH) variations, $F_\zeta(k)$, derived from SSH data from Topex/Poseidon altimeter measurements (Glazman, Fabrikant & Greysukh 1996; Glazman & Cheng 1999) taken over ocean regions dominated either by two-dimensional vortical turbulence or by BIG waves. For BIG waves one has the relation $k^2 F_L(\boldsymbol{k})/\omega(k)^2 = (\rho_* c^2)^{-1} U(\boldsymbol{k})$, where ρ_* is the mean water density and $U(\boldsymbol{k})$ is the potential energy spectrum. Thus, $U(\boldsymbol{k})$ may be extracted directly from altimeter measurements of SSH. In ocean regions dominated by BIG wave motions, the tracer spectrum, according to (2.10), should be similar to the SSH spectrum. A brief explanation of our data analysis approach is given in Appendix B.

Similarly to the simplified situation modelled in § 2.1, in which the tracer spectrum (2.14) contains two non-interacting components, the SSH spectrum is in general also a sum of two contributions – one due to BIG waves and the other due to two-dimensional vortical motions. These contributions can be separately extracted from SSH measurements by taking advantage of the fact that the characteristic time scales of these two components of ocean dynamics are vastly different (Gill 1982). The two-dimensional vortical motions are essentially quasi-geostrophic (QG), meaning that the horizontal pressure gradient is in an approximate instantaneous balance with the Coriolis force. This yields a simple scaling relationship between the kinetic and potential energy spectra: $U(\boldsymbol{k}) \sim k^{-2} F(\boldsymbol{k})$. Therefore, the SSH spectrum in regions dominated by QG motions should exhibit a rather steep spectral fall-off – between $k^{-11/3}$ and k^{-5} – corresponding, respectively, to the $k^{-5/3}$ and k^{-3} power laws relevant to the inertial ranges of the inverse energy and the direct enstrophy cascades. SSH spectra in BIG-wave-dominated regions are obtained by filtering out the slow component of SSH variability and retaining the fast, BIG-wave component. These spectra, in full accord with theoretical predictions (Glazman 1996), are much flatter: in mid- to low-latitude regions where BIG wave dynamics are dominated by the direct energy cascade, they fall off no faster than about $k^{-3/2}$; at high wavenumbers, $k \gg f/c$, where BIG waves are only weakly dispersive, the spectra fall off as $k^{-4/3}$; however, in higher-latitude regions in which the inverse cascade of BIG wave action dominates, the spectra fall off as rapidly as k^{-3} – but still slow in comparison to the eddy turbulence spectra of SSH variations. Theoretical and experimental spectra for all such situations are provided in Glazman (1996) and Glazman & Cheng (1999).

4.1. *Tracer fluctuations in regions of low eddy energy*

Let us consider cases expected to occur mainly in high-latitude regions such as that analysed in Gower *et al.* (1980) and reproduced in figure 1. In this region, ocean dynamics are dominated by BIG waves which are initially excited at the shortest scales (comparable to the local baroclinic Rossby radius of deformation – a few kilometres), and whose wave action is then transferred by weakly nonlinear wave–wave interactions to larger scales.

In figure 2 we show a theoretical SSH spectrum, based on analytic expressions in Glazman (1996) and Glazman & Cheng (1999), together with an altimeter-based analysis of SSH variations in a region south of Iceland. The two experimental curves correspond to separate spectra of fast (solid curve) and slow (dashed curve) components of the motion. The analysis directly confirms the proposed dominance

https://doi.org/10.1017/S0022112001006942 Published online by Cambridge University Press

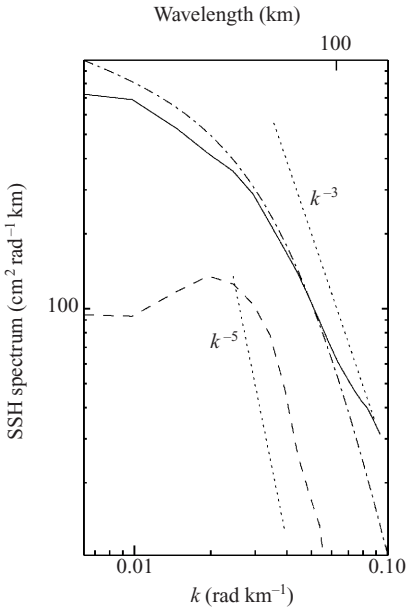


FIGURE 2. Theoretical and observed spectra of SSH variations (proportional to the potential energy spectrum, $U(k)$), dominated by the inverse cascade of BIG wave action, for a $10^\circ \times 10^\circ$ ocean area at about 60°N south of Iceland. Dash-dotted line: theoretical spectrum with computation based on that in Glazman (1996). The Kolmogorov constant α_P and wave action spectral flux rate P are selected such that $\alpha_P^{1/3} P \approx 3 \times 10^{-5}\,(\mathrm{m\,s^{-1}})^2$ to achieve the best match to the experimental data. Solid line: BIG-wave component of the observed spectrum of SSH variations along altimeter groundtracks. Dashed line: quasi-geostrophic (vortical) component of the observed SSH spectrum. A spectral peak near 250 km wavelength is consistent with the length of baroclinic Rossby waves in this region. Dotted straight lines are reference power laws. The k^{-5} line corresponds to the Kraichnan k^{-3} law for the two-dimensional turbulent kinetic energy spectrum in the inertial subrange of the direct cascade of enstrophy.

of BIG wave energy in this wavenumber range. The steep fall-off of the dashed line is in reasonable agreement with the k^{-5} power law (dotted line) corresponding to the inverse energy cascade of two-dimensional eddy turbulence. The solid curve falls off much more slowly, consistent with the discussion above. Thus, figure 2 confirms the theoretical prediction (2.10) and provides a compelling explanation of the chlorophyll spectrum in figure 1.

Due to intrinsic limitations of the altimeter measurements, the high-wavenumber range (wavelengths shorter than 50 km) of the SSH spectrum is distorted by measurement noise, so direct comparison with the data in figure 1 is not possible in this range. However, for studies of ocean dynamics and tracer fluctuations on larger scales – where effects of BIG wave turbulence should be particularly pronounced – altimeter data still provide valuable information. In order to estimate the tracer spectrum on scales greater than those explored by Gower *et al.* (1980) we shall employ a special technique of data analysis applicable to gappy and/or irregularly spaced satellite measurements over large ocean areas (Glazman *et al.* 1996). A brief description of the technique is presented in Appendix B.

Let us consider a case in which the relative level of two-dimensional turbulence is, again, low compared to that of BIG wave motions, and study tracer fluctuations on much larger scales than those in figure 1. One area in which QG motions are

https://doi.org/10.1017/S0022112001006942 Published online by Cambridge University Press

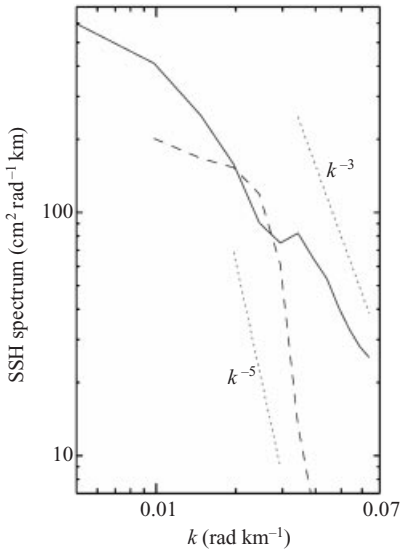


FIGURE 3. Altimeter-based one-dimensional spectra analogous to those in figure 2, but for an area of the northwest Pacific between 160° and 170°E and between 40° and 50°N. Notice a feature in the spectrum of BIG wave motions which agrees with the expected local peak due to semi-diurnal baroclinic tides in this region.

particularly weak is the northwestern Pacific. In figure 3 we show the spectra of SSH variations in this region. As in the case of figure 2, BIG wave motions indeed dominate SSH variations on almost all scales, except for a narrow range corresponding to wavelengths near 280 km. A small peak on the solid curve, at a wavelength of roughly 165 km, can be explained as a contribution from the semi-diurnal baroclinic tide – in accord with (3.8).

The two-dimensional and one-dimensional spectra of Chl-a fluctuations for this region are presented in figure 4. The important features of these spectra are the following. The overall behaviour of the one-dimensional spectrum is in reasonable agreement with the k^{-3} power law expected for BIG-wave-dominated variations of a tracer field. However, this inertial range is interrupted by an appreciable peak at about 310 km wavelength. Since this is the range where, according to figure 3, there is a large contribution of eddy motions, we conclude that this peak is due to an 'outcrop' of two-dimensional eddy turbulence on the generally stronger background of BIG wave motions. Finally, on scales starting at about 160 km we find relatively small local peaks, apparently caused by baroclinic tidal motions. These are in general agreement with the shape of the BIG wave spectrum in figure 3. We therefore conclude that the tracer spectrum agrees with that predicted by (2.14) for a case when the level of eddy turbulence, while not entirely negligible, is generally low in comparison to that of BIG wave turbulence.

4.2. *Tracer fluctuations in regions of intense eddy motions*

Gower *et al.* (1980) explained their observation of the k^{-3} spectrum as arising from two-dimensional eddy turbulence – the only kind of motion they expected in this region. In their critique, Lesieur & Sadourny (1981) pointed out that a theoretically justified spectrum, at the level of Kolmogorov-type dimensional analysis, is given by a k^{-1} power law. It was thought then that satellite-observed variations of chlorophyll

https://doi.org/10.1017/S0022112001006942 Published online by Cambridge University Press

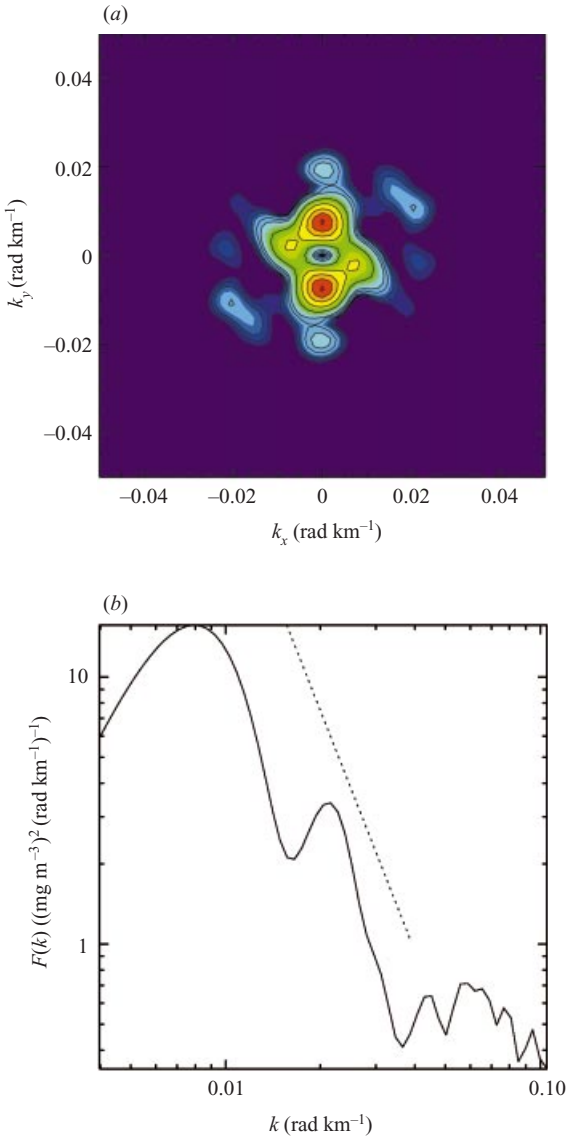


FIGURE 4. (*a*) Two-dimensional power spectrum of Chl-a fluctuations in the northwest Pacific region described in figure 3. (*b*) The one-dimensional spectrum corresponding to the two-dimensional spectrum in (*a*). The dotted line is the reference k^{-3} power law expected for BIG wave turbulence in the absence of eddy motions and baroclinic tides.

concentration in the ocean must be controlled by biological and light transmission factors rather than by fluid motion, a conclusion that we now argue against in this work. In this subsection we end by demonstrating that in regions dominated by well-developed two-dimensional eddy turbulence, chlorophyll fields *do* exhibit the behaviour consistent with the predictions of two-dimensional turbulence theory. Recent evidence for this behaviour was presented in Weichman & Glazman (1999) where we estimated one-dimensional spectra of chlorophyll fluctuations in a large ocean area east of Japan. There a highly intense Kuroshio current system generates strong eddies. Another region, also well known for an intense generation of two-

https://doi.org/10.1017/S0022112001006942 Published online by Cambridge University Press

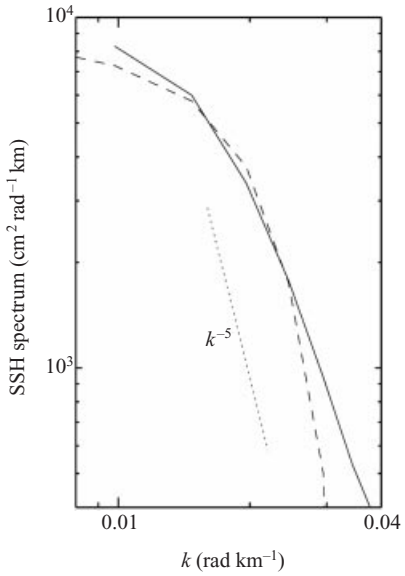


FIGURE 5. Altimeter-based one-dimensional spectra of SSH variations in an area of the Agulhas current shown in figure 8 (Appendix B). Solid curve: full spectrum, where no filtering of the SSH signal to separate slow (quasi-geostrophic) and fast (BIG wave) components has been performed. Dashed curve: filtered SSH component due only to quasi-geostrophic motions. The difference between these two curves would represent the spectrum of the fast, BIG wave motions. However, in this region this difference is well below the accuracy of the spectral analysis, and we therefore do not show it.

dimensional eddies (due to a large lateral shear in the ocean current field) is the Agulhas current region south of Africa. Figure 8 in Appendix B shows an actual Chlorophyll-a field observed by the SeaWiFS instrument. The one-dimensional SSH spectra of this field are shown in figure 5.

Since the level of eddy turbulence in these two regions is at least an order of magnitude greater than that in the north Atlantic and northwest Pacific regions treated earlier, the SSH variations on large spatial scales are almost entirely dominated by the QG component. Correspondingly, we find that the slow QG component is essentially indistinguishable from the full SSH spectrum, with the difference between the two being at the measurement noise level. In figure 5 we show therefore only the original one-dimensional spectrum of the instantaneous SSH field (solid curve) and the one-dimensional spectrum of its quasi-geostrophic component (dashed curve). As before, a reference k^{-5} power law, corresponding to the k^{-3} spectrum of two-dimensional eddy turbulence, is plotted for comparison. The two-dimensional spectrum of chlorophyll fluctuations is shown in figure 6, and the corresponding one-dimensional spectrum is shown in figure 7. The dominant peak in the latter – with the spatial scale near 400 km – is consistent with the size of the largest eddies known for this and for other dynamically similar regions (Best *et al.* 1999) in the Southern Ocean. On scales below about 100 km, the spectral fall-off, approximated by a k^{-1} power law (dashed line), agrees with that expected for a passive tracer in the two-dimensional eddy turbulence field governed by the direct cascade of enstrophy. However, two smaller peaks – at wavelengths of 157 and 78 km – may well be due to the semi-diurnal tides of the first and second baroclinic modes. As pointed out at the end of § 3, these tides are generated due to the presence of sharp variations in the local ocean floor topography.

https://doi.org/10.1017/S0022112001006942 Published online by Cambridge University Press

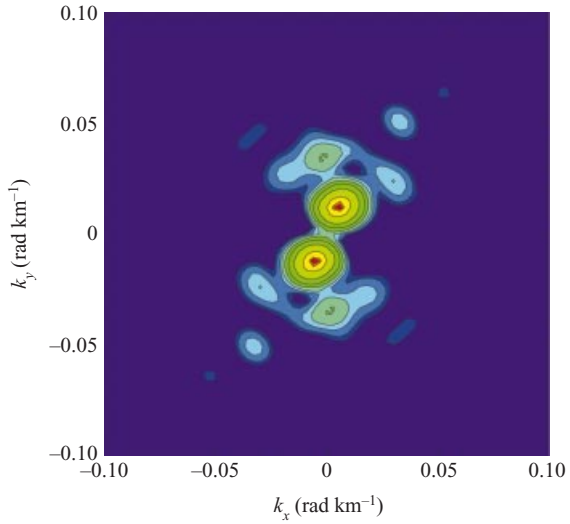


FIGURE 6. Two-dimensional power spectrum of Chlorophyll-a fluctuations in the Agulhas current region shown in figure 8 (Appendix B).

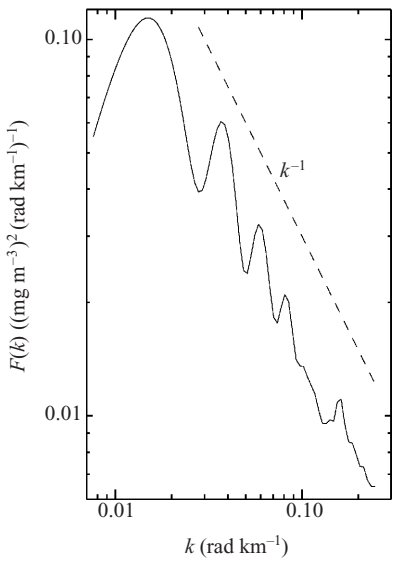


FIGURE 7. One-dimensional spectrum corresponding to the two-dimensional spectrum in figure 6. The dashed line represents a reference k^{-1} power.

In conclusion, the k^{-1} spectrum of tracer fluctuations is consistently observed in ocean regions dominated by two-dimensional eddy turbulence – in agreement with predictions of eddy turbulence theory.

Appendix A. Asymptotics of the spectral integral

Consider an integral of the form

$$I(r) = \int \frac{\mathrm{d}^d x}{x^{d+\sigma}} \exp(-(\boldsymbol{x}-\boldsymbol{r})^2/x^{\beta}), \tag{A 1}$$

with σ and β taking any real values. We divide the analysis into several cases.

https://doi.org/10.1017/S0022112001006942 Published online by Cambridge University Press

(i) If $\sigma < 0$ and $\beta < 2$, $I(r)$ remains finite as $r \to 0$, with the former ensuring convergence at small x and the latter ensuring convergence at large x. One then finds

$$I(0) = \int \frac{\mathrm{d}^d x}{x^{d+\sigma}} \exp(-x^{2-\beta}) = A_d \Gamma\left(\frac{-\sigma}{2-\beta}\right), \tag{A 2}$$

where $A_d = 2\pi^{d/2}/\Gamma(d/2)$ is the area of the unit sphere in d dimensions. One may then consider derivatives of $I(r)$ at $r = 0$. If $|\sigma|$ is large, the first few of these will in fact be finite. One finds, for example,

$$\left.\begin{aligned} I'(0) &= \int \frac{\mathrm{d}^d x}{x^{d+\sigma+\beta-1}} \exp(-x^{2-\beta}) \hat{\boldsymbol{r}} \cdot \hat{\boldsymbol{x}} = 0, \\ I''(0) &= \int \frac{\mathrm{d}^d x}{x^{d+\sigma+\beta}} \exp(-x^{2-\beta}) \left[-2 + 4x^{2-\beta} (\hat{\boldsymbol{r}} \cdot \hat{\boldsymbol{x}})^2\right] \\ &= -2A_d \Gamma\left(-\frac{\sigma+\beta}{2-\beta}\right) + \frac{4}{d} A_d \Gamma\left(1 - \frac{\sigma+\beta}{2-\beta}\right), \end{aligned}\right\} \tag{A 3}$$

and so on. The most singular term produced by each pair of derivatives effectively decreases $|\sigma|$ by β. This procedure therefore allows the first n Taylor coefficients of $I(r)$ to be computed, where n is the largest integer such that $2|\sigma| - n\beta$ is still positive. The $(n+1)$th derivative produces an integral whose most singular term produces a divergence at $r = 0$, i.e. an effective positive value of σ. This case is handled in (iii) below. The result is a subleading (but leading non-analytic) contribution to $I(r)$ given exactly by the last line of (A 4), but with $\sigma < 0$.

(ii) If $\sigma \geqslant 0$ and $\beta \leqslant 0$ (which includes the possibility that $\beta = 0$ could correspond to $\ln(1/x)$ behaviour), the singularity at small x makes $I(r)$ divergent for all values of r.

(iii) If $\sigma > 0$ and $0 < \beta < 2$, $I(r)$ is finite for any $r > 0$, but diverges as $r \to 0$ due to the singularity at small x. Making the substitution $\boldsymbol{u} = \boldsymbol{x}/r^{2/\beta}$ one obtains

$$\begin{aligned} I(r) &= \frac{1}{r^{2\sigma/\beta}} \int \frac{\mathrm{d}^d u}{u^{d+\sigma}} \exp(-(r^{2/\beta-1}\boldsymbol{u} - \hat{\boldsymbol{r}})^2/u^\beta) \\ &= \frac{1}{r^{2\sigma/\beta}} \int \frac{\mathrm{d}^d u}{u^{d+\sigma}} \exp(-1/u^\beta)[1 + o(1)] \\ &= \frac{A_d \Gamma(\sigma/\beta)}{r^{2\sigma/\beta}}[1 + o(1)], \end{aligned} \tag{A 4}$$

where $o(1)$ signifies neglected terms vanishing as $r \to 0$. The condition $\beta < 2$ is required so that $r^{2/\beta-1} \to 0$ as $r \to 0$ in the second line. One requires the inequality $\sigma > 0$ here for convergence at large u. If, pursuant to the discussion in (i), the divergent integral was obtained as the most singular term of the $(n+1)$th derivative of (A 2) with some initial value $\sigma_0 < 0$ (so that $\sigma = \sigma_0 + (n+1)\beta/2$), then reintegrating (A 4) $n+1$ times produces a subleading contribution with power law $r^{n+1-2\sigma/\beta} = r^{-2\sigma_0/\beta}$. Using the properties of the Γ-function it is elementary to show, as claimed in the last line of (i), that this term then takes exactly the form (A 4) with σ replaced by σ_0.

(iv) In the special case $\sigma = 0$ and $0 < \beta < 2$, $I(0)$ is still divergent due to the (now logarithmic) singularity at small x. This case is most simply treated by considering the limit $\sigma \to 0^-$. Equation (A 2) produces $I(0)$, while the leading power law correction

https://doi.org/10.1017/S0022112001006942 Published online by Cambridge University Press

can be obtained by examining the derivative

$$\begin{aligned}\frac{\mathrm{d}I(r)}{\mathrm{d}r} &= -\frac{2}{r^{1+2\sigma/\beta}}\int \frac{\mathrm{d}^d u}{u^{d+\sigma+\beta}}\exp(-(r^{2/\beta-1}\boldsymbol{u}-\hat{\boldsymbol{r}})^2/u^\beta)[1-\hat{\boldsymbol{r}}\cdot\boldsymbol{u}r^{2/\beta-1}]\\ &= -\frac{2}{r}\int \frac{\mathrm{d}^d u}{u^{d+\beta}}\exp(-1/u^\beta)[1+o(1)]\\ &= -\frac{2A_d\Gamma(1+\sigma/\beta)}{r^{1+2\sigma/\beta}}[1+o(1)]. \end{aligned} \tag{A 5}$$

Integrating this result produces a term in $I(r)$ varying as $r^{-2\sigma/\beta}$. Combining this with $I(0)$ we obtain

$$\begin{aligned} I(r) &= A_d\Gamma\left(\frac{-\sigma}{2-\beta}\right) - A_d\Gamma\left(\frac{\sigma}{\beta}\right)r^{-2\sigma/\beta}\\ &= 2A_d\Gamma(1+\sigma/\beta)\frac{1-r^{2\sigma/\beta}}{2\sigma/\beta} - \frac{A_d}{\sigma}\left[(2-\beta)\Gamma\left(1-\frac{\sigma}{2-\beta}\right)-\beta\Gamma\left(1+\frac{\sigma}{\beta}\right)\right]. \end{aligned} \tag{A 6}$$

Taking the limit $\sigma \to 0$, the first term produces a logarithm, while the last term produces the finite result $2A_d\Gamma'(1) = 2A_d\psi(1) = -2A_dC$, where $C = 0.577215\ldots$ is Euler's constant. Thus for $\sigma = 0$ and $0 < \beta < 2$ we finally obtain

$$I(r) = 2A_d[\ln(1/r) - C] + o(1). \tag{A 7}$$

(v) If $\beta > 2$ the integral defining $I(0)$ is convergent at small x for any value of σ, positive or negative. If $\sigma > 0$ the integral is convergent at large x as well and (A 2) remains valid. However, if $\sigma \leqslant 0$ the integral fails to converge at large x. Physically, however, this is an artifact of the power law approximation for $\gamma(x)$, which must saturate to a finite value at $x \simeq \xi$, ξ being the correlation radius of the wave field. With this cutoff, for $\sigma \leqslant 0$ one finds a strong cutoff-dependent $I(0) \sim [1-\xi^{-\sigma}]/\sigma$ [$\sim \ln(\xi)$ for $\sigma = 0$].

(vi) In the special case $\beta = 2$ the integral defining $I(0)$ is convergent at small x if $\sigma < 0$ but is divergent at large x. One again obtains the cutoff-dependent result $I(0) \sim [1-\xi^{-\sigma}]/\sigma$. Derivatives with respect to r again increase the effective value of σ, and the discussion in (i) is relevant to the extraction of the leading singular term which arises when this effective value first becomes positive. If $\sigma > 0$, $I(0)$ is now convergent at large x but divergent at $x = 0$. The substitution $\boldsymbol{u} = \boldsymbol{x}/r$ then yields the *exact* power law form

$$I(r) = \frac{1}{r^\sigma}\int \frac{\mathrm{d}^d u}{u^{d+\sigma}}\exp(-(\boldsymbol{u}-\hat{\boldsymbol{r}})^2/u^2). \tag{A 8}$$

Using the result that the angular average of $\mathrm{e}^{\mathrm{i}\boldsymbol{k}\cdot\hat{\boldsymbol{x}}}$ over all directions $\hat{\boldsymbol{x}}$ is given by

$$\langle \mathrm{e}^{\mathrm{i}\boldsymbol{k}\cdot\hat{\boldsymbol{x}}}\rangle_{\hat{\boldsymbol{x}}} = \Gamma(d/2)(2/k)^{(d-2)/2}J_{(d-2)/2}(k), \tag{A 9}$$

we obtain, with $\mathrm{i}k \to 1/u$,

$$\begin{aligned} I(r) &= \frac{(2\pi\mathrm{i})^{d/2}}{\mathrm{i}\mathrm{e}r^\sigma}\int_0^\infty \frac{\mathrm{d}u}{u^{1+\sigma}}u^{(d-2)/2}J_{(d-2)/2}(1/\mathrm{i}u)\mathrm{e}^{-1/u^2}\\ &= \frac{\Gamma(\sigma/2)\pi^{d/2}}{\mathrm{e}\Gamma(d/2)}{}_1F_1(\sigma/2, d/2, 1/4)\frac{1}{r^\sigma}, \end{aligned} \tag{A 10}$$

where in the last line relation 6.631.1 (p. 716) in Gradshteyn & Rhyzhik (1981)

https://doi.org/10.1017/S0022112001006942 Published online by Cambridge University Press

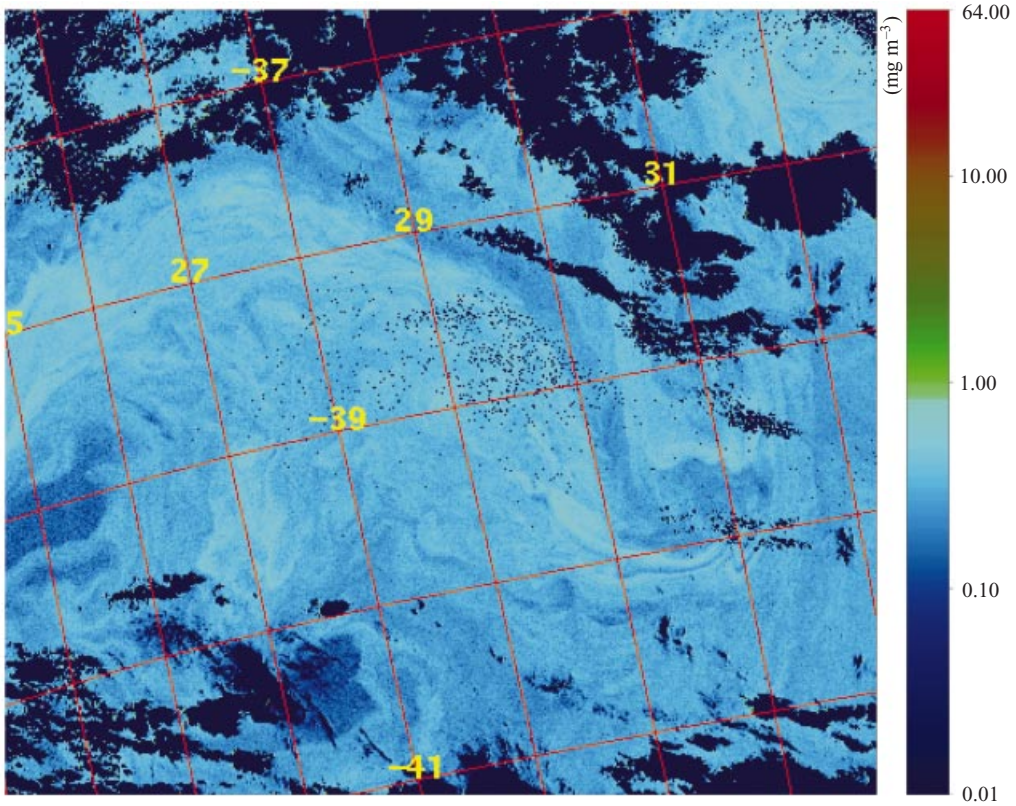


FIGURE 8. Chlorophyll-a concentration observed by SeaWiFS on September 1, 1998 in the Agulhas current region (south of Africa).

has been used. Finally, if $\sigma = 0$, $I(r)$ contains a logarithmic divergence at large x. Applying a cutoff at $x = \xi$, one obtains

$$I(r) = \int_{u<\xi/r} \frac{\mathrm{d}^d u}{u^d} \exp(-(\boldsymbol{u} - \hat{\boldsymbol{r}})^2/u^2)$$
$$= A_d \int_1^{\xi/r} \frac{\mathrm{d}u}{u} + O(1) = A_d \ln(\xi/r) + O(1), \qquad \text{(A 11)}$$

where the $O(1)$ correction depends on the detailed implementation of the cutoff.

Appendix B. Estimation of Chl-a and SSH spectra

Ocean tracer distributions, such as sea surface temperature or chlorophyll-a concentration fields, are measured from space by passive infrared and visible-light imaging sensors. We shall analyse the data on chlorophyll concentration from the Sea-viewing Wide Field-of-view Sensor (SeaWiFS) instrument launched in 1997. These measurements are available with spatial resolutions as high as 1.3 km. Since atmospheric clouds are present over any sufficiently large ocean area, satellite images always have gaps. One such image, of an ocean region about 500 km south of the southern tip of Africa, is shown in figure 8. Black areas are clouds or otherwise missing data. The strong Agulhas current and its retroflection create a highly intense eddy field.

In order to estimate the power spectrum of Chl-a fluctuations we first subtract the

https://doi.org/10.1017/S0022112001006942 Published online by Cambridge University Press

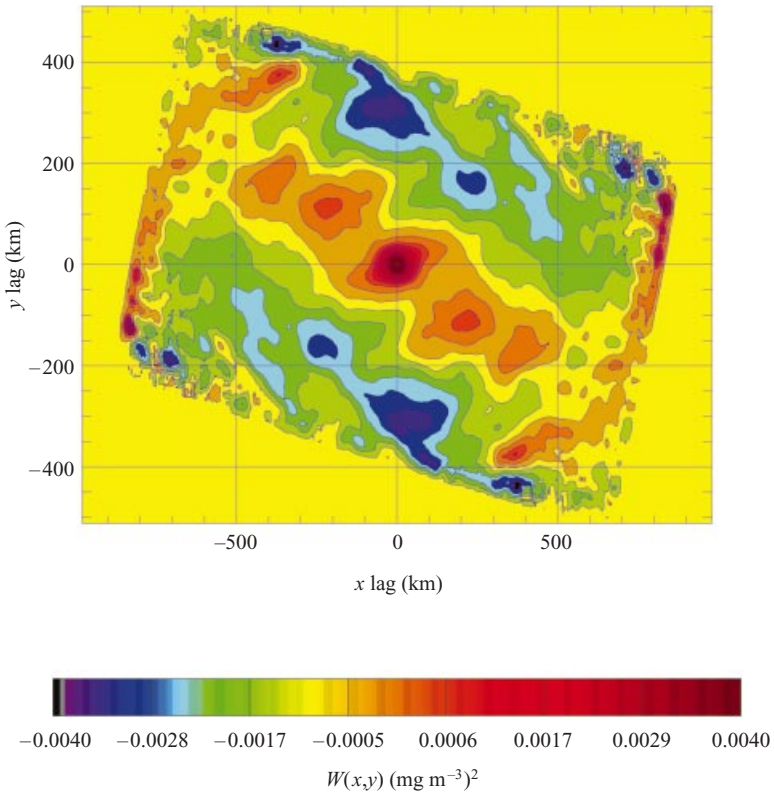


FIGURE 9. Two-dimensional spatial autocorrelation function of Chlorophyll concentration fluctuations in the area shown in figure 8.

mean value of Chl-a concentration from the value at each point, and then compute products of the differences, $q(\boldsymbol{x})q(\boldsymbol{x}')$, for all pairs of points $\boldsymbol{x}$ and $\boldsymbol{x}'$. These products are binned in 4 km × 4 km two-dimensional cells of the spatial lag $\boldsymbol{x} - \boldsymbol{x}'$, and finally averaged within each bin to yield an estimate of the spatial autocorrelation function $R(\boldsymbol{x} - \boldsymbol{x}')$ (equation (1.2)). The autocorrelation function obtained by this method for the Agulhas current region, figure 8, is shown in figure 9. The power spectrum is obtained as the two-dimensional Fourier transform of $R(\boldsymbol{x} - \boldsymbol{x}')$. The Hanning window is employed to reduce the adverse effects of the finite size of the geographic area and of the spatial inhomogeneity of the Chl-a field on the largest scales. The two-dimensional power spectrum corresponding to figure 9 is shown in figure 6.

A detailed description of our altimeter data analysis technique is presented in Glazman *et al.* (1996) and Glazman & Cheng (1999). Here we explain only the key feature, namely the separation of the observed SSH spectrum into two components corresponding to slow (quasi-geostrophic) and fast (inertia–gravity wave) motions. The Topex/Poseidon satellite altimeter takes SSH measurements every 6.4 km along its one-dimensional groundtracks on both descending and ascending passes over any given ocean area. Within any 10 day interval (the orbit repeat cycle), it covers the world ocean with a grid of groundtracks, yielding SSH values $\zeta(\boldsymbol{x}, t)$ at points $\boldsymbol{x}$ along the ground tracks. Within a limited surface area, say 10° × 10°, we thus obtain a set of $\zeta(\boldsymbol{x}, t)$ with time differences from zero (for measurements taken on individual grountrack passes) to ten days (for measurements taken on different passes within a

https://doi.org/10.1017/S0022112001006942 Published online by Cambridge University Press

repeat cycle). Accumulating all such measurements over a sufficiently long (on the time scale of QG motions) interval (e.g. six months) we then estimate the spatio–temporal autocorrelation function of SSH variations, $W(\boldsymbol{r}, \tau)$, where $\boldsymbol{r}$ and τ are the two-dimensional spatial and one-dimensional time lags, repectively. The contribution of the fast, BIG wave component, of this function vanishes for τ greater than the characteristic autocorrelation time of BIG wave oscillations, t^*_{BIG} (a few dominant BIG wave periods). Thus, $W(\boldsymbol{r}; \tau \geqslant t^*_{\mathrm{BIG}})$ is determined solely by the QG motions. Because the characteristic time scale of variations of the two-dimensional vortical velocity field is much greater than t^*_{BIG}, the function $W(\boldsymbol{r}, \tau = t^*_{\mathrm{BIG}})$ is essentially indistinguishable from the equal time spatial autocorrelation function of the QG component. Its spatial Fourier transform yields the wavenumber spectrum of QG motions.

For all practical purposes, altimeter measurements on individiual passes can be viewed as instantaneous because the satellite covers a 3000 km ground distance in three minutes. Therefore, one-dimensional spectra of SSH variations along a single pass contain contributions of both fast and slow components of SSH variability. If we now reduce the two-dimensional spectrum obtained earlier to a one-dimensional form and subtract it from the one-dimensional spectrum of the along-track SSH variations, the difference yields an estimate of the spectrum of fast motions. It is this spectrum that is plotted as a solid curve in figures 2 and 3.

We thank L. Piterbarg, A. Balk, and R. McLaughlin for useful discussions. Part of this work was performed at the Jet Propulsion Laboratory, California Institute of Technology, under contract with the National Aeronautics and Space Administration. The authors also thank the SeaWiFS project and the Distributed Active Archive Center at the Goddard Space Flight Center for the SeaWiFS data used in this work.

REFERENCES

Barale V. & Trees, C. C. 1987 Spatial variability of the ocean color field in CZCS imagery. *Adv. Space Res.* **7**(2), 95–100.

Batchelor, G. K. 1969 Computation of the energy spectrum in homogeneous two-dimensional turbulence. *Phys. Fluids Suppl.* **2**, 233–238.

Bennett, A. F. 1996 Particle displacements in inhomogeneous turbulence. In *Stochastic Modelling in Physical Oceanography* (ed. R. Adler, P. Muller & B. Rozovskii), pp. 1–45. Birkhauser.

Best, S. E., Ivchenko, V. O., Richards, K. J., Smith, R. D. & Malone, R. C. 1999 Eddies in numerical models of the Antarctic Circumpolar Current and their influence on the mean flow. *J. Phys. Oceanogr.* **29**, 328–350.

Charney, J. G. 1971 Geostrophic turbulence. *J. Atmos. Sci.* **28**, 1087–1095.

Cipollini, P., Cromwell, D., Challenor, P. G. & Raffaglio, S. 2001 Rossby waves detected in global ocean colour data. *Geophys. Res. Lett.* **28**, 323–326.

Denman, K. L. & Abbott, M. R. 1994 Time scales of pattern evolution from cross-spectral analysis of advanced very high resolution radiometer and coastal zone color scanner imagery. *J. Geophys. Res.* **99**, 7433–7442.

Deschamps, P. Y., Frouin, R. & Wald, L. 1981 Satellite determination of the mesoscale variability of the sea surface temperature. *J. Phys. Oceanogr.* **11**, 864–870.

Gavrilin, B. L., Mirabel, A. P. & Monin, S. A. 1972 On the energy spectrum of synoptic processes. *Izv. Atmos. Ocean Phys.* **8**(5), 483–493.

Gill, A. E. 1982 *Atmosphere-Ocean Dynamics.* Academic.

Glazman, R. E. 1996 Spectra of baroclinic inertia-gravity wave turbulence. *J. Phys. Oceanogr.* **26**, 1256–1265.

Glazman, R. E. & Cheng, B. 1999 Altimeter observations of baroclinic oceanic inertia-gravity wave turbulence. *Proc. R. Soc. Lond.* A **455**, 91–123.

https://doi.org/10.1017/S0022112001006942 Published online by Cambridge University Press

Glazman, R. E., Fabrikant, A. & Greysukh, A. 1996 Statistics of spatio-temporal variations of sea surface height based on Topex altimeter measurements. *Intl J. Rem. Sens.* **17**, 2647–2666.

Gower, J. F. R., Denman K. L. & Holyer, R. J. 1980 Phytoplankton patchness indicates the fluctuation spectrum of mesoscale oceanic structure. *Nature* **288**, 157–159.

Gradshteyn, I. S. & Rhyzhik I. M. 1981 *Table of Integrals, Series, and Products.* Academic.

Herterich, K. & Hasselmann, K. 1982 The horizontal diffusion of tracers by surface waves. *J. Phys. Oceanogr.* **12**, 704–711.

Klyatskin, V. I. 1994 Statistical description of diffusing tracers in random velocity fields. *Phys.-Uspekhi* **37**(5), 501–514.

Kraichnan, R. H. 1967 Inertial ranges in two-dimensional turbulence. *Phys. Fluids* **10**, 1417–1428.

Kraichnan, R. H. 1971 Inertial range transfer in two- and three-dimensional turbulence. *J. Fluid Mech.* **47**, 525–535.

Kraichnan, R. H. 1974 Convection of a passive scalar by a quasi-uniform random straining field. *J. Fluid Mech.* **64**, 737–762.

Kubo, R. 1963 Stochastic Liouville equations. *J. Math. Phys.* **4**, 174–183.

Lesieur, M. & Sadourny, R. 1981 Satellite-sensed turbulent ocean structure. *Nature* **294**, 673.

Maltrud, M. E., Smith, R. D., Semtner, A. J. & Malone, R. C. 1998 Global eddy-resolving ocean simulations driven by 1985–1995 atmospheric winds. *J. Geophys. Res.* **103**, 30825–30853.

Monin, A. S. & Yaglom, A. M. 1971 *Statistical Fluid Mechanics*, Vol. 1, MIT Press.

Ogura, Y. 1952 The theory of turbulent diffusion in the atmosphere. *J. Met. Soc. Japan* **30**, 53–58.

Ogura, Y. 1962 Energy transfer in a normally distributed and isotropic turbulent velocity field in two dimensions. *Phys. Fluids* **5**, 395–401.

Piterbarg, L. I. 1997 Short-correlation approximation in models of turbulent diffusion. In *Stochastic Models in Geosystems* (ed. S. A. Molchanov & W. A. Wojczinski), pp. 313–352. Springer.

Saunders, P. M. 1972 Comments on wavenumber-frequency spectra of temperature in the free atmosphere. *J. Atmos. Sci.* **29**, 197–199.

Uz, B. M., Yoder, J. A. & Osychny, V. 2001 Pumping of nutrients to ocean surface waters by the action of propagating planetary waves. *Nature* **409**, 597–600.

Weichman, P. B. & Glazman, R. E. 1999 Turbulent fluctuation and transport of passive scalars by random wave fields. *Phys. Rev. Lett.* **83**, 5011–5014.

Weichman, P. B. & Glazman, R. E. 2000 Passive scalar transport by travelling wave fields. *J. Fluid Mech.* **420**, 147–200.

https://doi.org/10.1017/S0022112001006942 Published online by Cambridge University Press